Novel signals for the type-X two-Higgs-doublet scenario at the Large Hadron Collider

Biswarup Mukhopadhyaya,[*] Sirshendu Samanta,[†] Tousik Samui,[‡] and Ritesh K. Singh[§]

Department of Physical Sciences, Indian Institute of Science Education and Research Kolkata, Mohanpur, 741246, India

(Received 16 June 2023; accepted 11 September 2023; published 6 October 2023)

We consider, in the context of the Large Hadron Collider, some signals of the type-X two Higgs doublet model (2HDM). The analysis takes into account all theoretical and observational constraints, and is based on the final state comprising a same-sign dilepton pair and a pair of same-sign τ jets. The crucial ingredient in making the signal clean is the same-sign feature of both the dilepton and the τ-jet pair individually. After a detailed estimate of the signal and all noteworthy backgrounds, we show that this channel offers by far the best signal significance among those studied so far, predicting discovery with an integrated luminosity of 3000 fb^{-1}, and strong indications even with 1000 fb^{-1} if systematic uncertainties do not exceed about 10%. We also demonstrate that the recently developed dynamic radius jet algorithm is effective in this connection.

DOI: 10.1103/PhysRevD.108.075004

I. INTRODUCTION

Whether more than one scalar $SU(2)$ doublets are responsible for the still enigmatic phenomenon of electroweak symmetry breaking (EWSB) continues to remain an open issue. One reason behind this is the repetitive occurrence of spin-$1/2$ fields, and the unanswered query as to why scalar fields in the electroweak (EW) theory should be immune to such repetition. Thus there remains continued interest in two Higgs doublet models (2HDM) [1,2], the simplest examples of an extended scalar sector. Such scenarios are consistent with electroweak precision tests (EWPT), and, in spite of the data on the 125-GeV scalar suggesting closeness to the "alignment limit" [3], the potential for new phenomenology is quite rich. Such prospects, however, depend on what type of 2HDM it is. Since the unconstrained coupling of both the doublets to $T_3 = +1/2$ as well as $-1/2$ fermions can lead to tree-level flavor violation, a frequent practice is to impose $\mathbb{Z}_2$ symmetries on the Yukawa terms in various ways, so that each fermion couples to one doublet only. One thus ends up with models belonging to type-I, type-II, type-X or lepton-specific and flipped type [1,2]. The experimental signatures, too, depend on which type one is concerned with. This happens essentially because of different patterns of Yukawa interactions in the different models. It is therefore imperative to find out about distinctive signals of each kind of 2HDM, since the probability of Nature choosing any one of them is *prima facie* the same. We are concerned with some signals of the type-X 2HDM in this paper.

It is also worth mentioning that, for $m_A \lesssim 100$ GeV, this model contributes [4,5] substantially to the anomalous magnetic moment $(g-2)$ of the muon, where an apparent excess in the measured value over the standard model (SM) has been reported over the years [6–8]. On the other hand, some lattice calculations of the hadronic vacuum polarization contribution [9–14] claim that the SM deficit is actually taken care of. Nonetheless, one has to remain alert to the contributions in Type-X 2HDM, since uncertainties in long-distance QCD are not entirely removable. Muon $(g-2)$ can also act as a piece of data constraining any electroweak scenario contributing to it. We have included this piece of data in our parameter scan of type-X 2HDM, for selecting our benchmark points.

It is thus important to closely examine the predictable signals of type-X 2HDM at the Large Hadron Collider (LHC), particularly when the high-luminosity run takes place [15]. Though some earlier studies have partially constrained the parameter space [16], one needs to proactively devise search strategies using various final states pertaining to this particular model, where a considerable scope for improvement remains is still there.

[*]biswarup@iiserkol.ac.in
[†]ss21rs027@iiserkol.ac.in
[‡]tousiksamui@gmail.com
[§]ritesh.singh@iiserkol.ac.in

Studies have taken place, suggesting reconstruction of A in the $\mu^+\mu^-$ channel[1] [23]. It is also important to find signatures of the heavier neutral and charged scalars $H, H^\pm$. For this, the muonic channel of at least one A which results from decays of the heavier states have been made use of [24]. Although this results in apparently clean signals, rates are suppressed by the $A \to \mu^+\mu^-$ branching ratio, thus making it difficult to rise above the 3σ-level with an integrated luminosity of 3000 fb^{-1}.

We go beyond these studies and consider instead 4τ signals which arise, for example, via the hard scattering channels $pp \to HA, H^\pm A$, followed by $H \to ZA$ and $H^\pm \to W^\pm A$. Each of the two A's thus produced decays dominantly to a τ pair. The novelty of our approach lies in the following points:

(i) The events corresponding to charged and neutral heavy scalars can be clubbed together since their masses are constrained to be small from electroweak precision observables. Moreover, we analyse events where the Z or the W decays into jets.

(ii) Out of the 4τ final state, we have concentrated on events where two same-sign τ's have one-and three-prong hadronic decays, while the remaining τ-pair, also of the same sign, decay leptonically. In order to do so, we have utilized the claim that the τ-induced jets can have charge identification efficiencies of 99% and 70% in the one-and three-prong channels, respectively [25]. Thus one looks for a pair of same-sign leptons as well as a pair of same-sign tau-jets. After convolution with the appropriate tau-identification efficiencies, and on using suitable event selection criteria, one thus ends up with substantial signal rates along with a rather impressive background reduction.

(iii) In addition to the decays $H \to ZA$, we have included cases where the H directly decays into a τ-pair, thus yielding events similar to those mentioned above. The additional jets arise from showering. This inclusion boosts the strength of the signal.

(iv) We have used a recently developed dynamic radius jet algorithm [26] which is demonstrated to be as good as the anti-k_t algorithm.

The paper is organized as follows. A brief outline of the type-X 2HDM has been provided in Sec. II, together with the existing constraints on the parameter space. The choice of benchmarks for our analysis is thus motivated. Section III A contains a full-length discussion of the proposed signal and its various backgrounds, which leads to the adopted event selection strategy. The results are presented and discussed in Sec. III B. We summarize and conclude in Sec. IV.

[1] It should be noted that the best signal significance in this channel was predicted for $m_A < m_h/2$, which has subsequently been disfavored by the data in $h \to 4\tau$ [4,5,17–22].

II. TYPE-X 2HDM: PARAMETERS AND CONSTRAINTS

As has been already mentioned, type-X 2HDM envisions a situation where, in the Higgs flavor basis, Φ_2 has Yukawa interactions with all quarks, and Φ_1, with leptons. This is ensured by imposing a $\mathbb{Z}_2$ symmetry on the Yukawa interaction, under which the fields transform as

$$\Phi_1 \to -\Phi_1; \qquad \Phi_2 \to \Phi_2; \tag{1}$$

$$Q_L, Q_R, L_L \to Q_L, Q_R, L_L; \qquad L_R \to -L_R, \tag{2}$$

where the subscripts L, R stand for left and right-chiral projections, respectively.

The scalar potential, neglecting CP-violation, is given by

$$\begin{aligned} V_{\mathrm{scalar}} = {} & m_{11}^2 \Phi_1^\dagger \Phi_1 + m_{22}^2 \Phi_2^\dagger \Phi_2 + \lambda_1 (\Phi_1^\dagger \Phi_1)^2 + \lambda_2 (\Phi_2^\dagger \Phi_2)^2 \\ & + \lambda_3 (\Phi_1^\dagger \Phi_1)(\Phi_2^\dagger \Phi_2) + \lambda_4 (\Phi_1^\dagger \Phi_2)(\Phi_2^\dagger \Phi_1) \\ & + \left\{ -m_{12}^2 \Phi_1^\dagger \Phi_2 + \frac{\lambda_5}{2} (\Phi_1^\dagger \Phi_2)^2 + \mathrm{H.c.} \right\}, \end{aligned} \tag{3}$$

It should be noted that the $\mathbb{Z}_2$ is broken above by the soft term proportional to m_{12}^2 which does not reintroduce flavor violation at the tree level. After the spontaneous EWSB, the two Higgs doublets acquire vacuum expectation values (vevs) v_1 and v_2, which usually are reparametrize as $v = \sqrt{v_1^2 + v_2^2}$ and $\tan\beta = v_2/v_1$. In terms of these parameters and the neutral scalar mixing angle α, it is possible to express the physical masses of the spin-0 particles, namely h, H (the neutral scalars), A (the neutral pseudoscalar) and $H^\pm$ (the charged scalars):

$$m_H^2 = M^2 s_{\alpha-\beta}^2 + \left(\lambda_1 c_\alpha^2 c_\beta^2 + \lambda_2 s_\alpha^2 s_\beta^2 + \frac{\lambda_{345}}{2} s_{2\alpha} s_{2\beta} \right) v^2, \tag{4}$$

$$m_h^2 = M^2 s_{\alpha-\beta}^2 + \left(\lambda_1 s_\alpha^2 c_\beta^2 + \lambda_2 c_\alpha^2 s_\beta^2 - \frac{\lambda_{345}}{2} s_{2\alpha} s_{2\beta} \right) v^2, \tag{5}$$

$$m_A^2 = M^2 - \lambda_5 v^2, \tag{6}$$

$$m_{H^\pm}^2 = M^2 - \frac{\lambda_4 + \lambda_5}{2} v^2, \tag{7}$$

where $M^2 = m_{12}^2/(s_\beta c_\beta)$ and, for an angle θ, $s_\theta (c_\theta)$ represents $\sin\theta (\cos\theta)$. Finally, once the scalar, pseudoscalar and charged scalar mass matrices are diagonalized and the Goldstone bosons are separated out, the Yukawa interactions of the various mass eigenstates are given by

TABLE I. Scale factors of the SM fermion couplings to the 2HDM physical scalars.

$\xi_u^h = \xi_d^h$	ξ_ℓ^h	$\xi_u^H = \xi_d^H$	ξ_ℓ^H	$\xi_u^A = -\xi_d^A$	ξ_ℓ^A
$\frac{\cos\alpha}{\sin\beta}$	$-\frac{\sin\alpha}{\cos\beta}$	$\frac{\sin\alpha}{\sin\beta}$	$\frac{\cos\alpha}{\cos\beta}$	$\cot\beta$	$\tan\beta$

$$\mathcal{L}_{\text{Yukawa}} = -\sum_f \frac{m_f}{v}(\xi_f^h \bar{f} f h + \xi_f^H \bar{f} f H - i\xi_f^A \bar{f}\gamma_5 f A) - \frac{\sqrt{2}}{v}[V_{ud}^{\text{CKM}}(m_u \xi_u^A \bar{u}_R d_L + m_d \xi_d^A \bar{u}_L d_R) H^+ + m_\ell \xi_\ell^A \bar{\nu}_L \ell_R H^+ + \text{H.c.}], \quad (8)$$

The case-by-case details of these couplings for various fermions are summarized in Table 1.

For the current analysis, we have implemented the model in the *Mathematica*-based package SARAH [27,28] to generate UNIVERSAL FEYNRULES OUTPUT (UFO) [29] and SPHENO [30,31] compatible output. The SPHENO is then used to generate a spectrum with masses and couplings for a given input parameter point.

In this study, h is identified as the observed 125 GeV scalar at the LHC [32,33]. The other CP-even physical scalar H is kept heavier than h. The well-measured masses of the gauge bosons, namely W and Z bosons, are controlled by vev (v). This fixes the value of v at 246 GeV [34]. The remaining parameters in the scalar sector are treated as free, subject to constraints from theoretical considerations and experimental measurements. The following constraints are relevant here:

Theoretical constraints The electroweak symmetry breaking minimum for the scalar potential corresponds to a stable vacuum, provided [35,36]

$$\lambda_{1,2} > 0, \qquad \lambda_3 > -\sqrt{\lambda_1\lambda_2}, \quad \text{and} \quad \lambda_3 + \lambda_4 - |\lambda_5| > -\sqrt{\lambda_1\lambda_2}.$$

Furthermore, we restrict the model to satisfy the perturbative unitary constraints. All the quartic couplings, therefore, should satisfy $|\lambda_i| < 4\pi$, ($i = 1, 2, \ldots, 6$), in order for the Lagrangian to be perturbative. Further, tree-level unitarity in any scalar-scalar to scalar-scalar scattering demands that the real part of each term in the partial wave decomposition of $2 \to 2$ scattering amplitude should be smaller than $1/2$. This leads to the following conditions on the λ parameters [2,37,38]:

$$a_\pm = \frac{3}{2}(\lambda_1 + \lambda_2) \pm \sqrt{\frac{9}{4}(\lambda_1 - \lambda_2)^2 + (2\lambda_3 + \lambda_4)^2} \le 8\pi, \quad (9)$$

$$b_\pm = \frac{1}{2}(\lambda_1 + \lambda_2) \pm \sqrt{\frac{1}{4}(\lambda_1 - \lambda_2)^2 + \lambda_4^2} \le 8\pi, \quad (10)$$

$$c_\pm = \frac{1}{2}(\lambda_1 + \lambda_2) \pm \sqrt{\frac{1}{4}(\lambda_1 - \lambda_2)^2 + \lambda_5^2} \le 8\pi, \quad (11)$$

$$e_\pm = \lambda_3 + 2\lambda_4 \pm 3\lambda_5 \le 8\pi, \quad (12)$$

$$f_\pm = \lambda_3 \pm \lambda_4 \le 8\pi, \quad (13)$$

$$g_\pm = \lambda_3 \pm \lambda_5 \le 8\pi, \quad (14)$$

where $a_\pm, b_\pm, \ldots, g_\pm$ are the eigenvalues of the scattering amplitude matrices involving all possible $2 \to 2$ scalar-scalar scattering.

Higgs properties and scalar searches In this model, the properties of the 125 GeV scalar are bound to deviate from predictions of the SM. Although the measured values of its couplings are almost consistent with the SM prediction, there is a small window in the experimental measurement where new physics can be accommodated. This, in turn, restricts the parameters of any given model. Also, searches for the additional scalars yield upper limits on their production cross section. Constraints thus arising are included in publicly available packages called HiggsSignals [39] and HiggsBounds [40,41], which restrict the parameter space of the model in consideration.

Oblique electroweak parameters The precision measurement of the electroweak observables has widely been studied at the Large Electron Positron (LEP) collider. The essence of these lies in the Peskin–Takeuchi parameters, namely S, T, and U [42,43]. In type-X 2HDM, the values U parameter is known to be very small. In the limit $U = 0$, the current measured values are $S = -0.01 \pm 0.07$ and $T = 0.04 \pm 0.06$ with a 92% correlation between them [34]. We used the covariance matrix in the $S - T$ plane to calculate χ^2 after the calculation of S and T at one-loop using SPHENO [30,31] for each parameter point. The parameter points are then subject to passing the constraint at the 90% C.L.

We have performed a thorough scan of the parameters subject to the above constraints. For the scan, the six parameters, namely λ_1, m_{12}, m_H, $m_{H^\pm}$, m_A, $\tan\beta$, some of which can be traded off with the quartic couplings in the Lagrangian given in Eq. (3), have been varied in the following range:

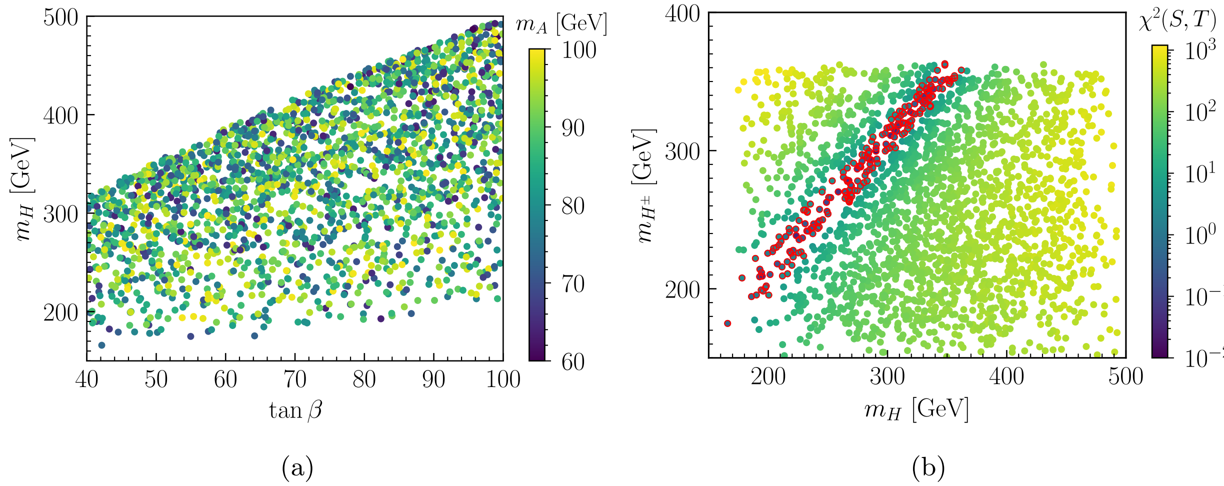

FIG. 1. (a) Scatter plot of m_H vs. $\tan\beta$ allowed by HiggsSignals [39] and HiggsBounds [40,41]. The different colors on the points represent the variation of the m_A. The upper limits of m_H and $m_{H^\pm}$ are because of the chosen range of m_{12}^2 for the scan. (b) Scatter plot of m_H vs. $m_{H^\pm}$ allowed by HiggsSignals and HiggsBounds. The points with red circles are allowed by the measurement of EW oblique parameter S and T parameter at 90% C.L. [34]. The colors of the points represent the value of $\chi^2(S,T)$.

$$m_H \in (150, 500)\ \text{GeV}, \qquad m_{H^\pm} \in (150, 350)\ \text{GeV}, \qquad m_A \in (60, 100)\ \text{GeV},$$
$$\tan\beta \in (40, 100), \qquad m_{12}^2 \in (450, 2500)\ \text{GeV}^2, \quad \text{and} \quad \lambda_1 = 0.1. \tag{15}$$

The coupling constant λ_1 appears as $\lambda_1 v_1^2$ in the neutral scalar mass matrix. In our setup, $\tan\beta = v_2/v_1 \gg 1$, and, therefore, the mass and mixing angles are almost independent of the value λ_1. Since our analysis is mostly unaffected by the exact value of this constant, we have kept λ_1 constant, with an illustrative value of 0.1.

In Figure 1, we show the allowed parameter points that satisfy the above constraints. The points on the $\tan\beta$ and m_H plane in Fig. 1(a) are allowed by theoretical and experimental limits. The feature of having upper limits (approximately linear in $\tan\beta$) of m_H and $m_{H^\pm}$ is due to the restriction of the parameter m_{12}^2. The lower limit on m_{12}^2 is to avoid making various physical masses (m_A, $m_{H^\pm}$) too small to satisfy phenomenological constraints, while the upper limit confines one to regions where the extended scalar sector lies within the LHC. The scatter plot in Fig. 1(b) shows the allowed points in the $m_H - m_{H^\pm}$ plane. The red circled points are after the imposition of constraints from the oblique parameters S and T. This restricts the mass splitting between H and $H^\pm$ to small values.

In the high $\tan\beta$ limit and alignment limit ($\beta - \alpha \simeq \pi/2$), the couplings of the quarks to the SM-like Higgs boson are very similar to the SM Higgs. On the other hand, the couplings of the additional Higgs bosons, namely $H^\pm$, H, and A, to any quarks or vector bosons, are suppressed by $1/\tan\beta$ in the type-X 2HDM setup. Therefore, the new physics contribution of these additional scalars, via the loops, to the low energy processes like quark flavor violating processes is negligible. Hence the type-X 2HDM model is mostly unconstrained from quark flavor-violating observations.

Finally, we take into account the numerical requirements for explaining $(g-2)_\mu$ which serves as a motivation for type-X 2HDM [6–8]. Originally, a scenario with $m_A \approx 30$–40 GeV, consistently with all phenomenology, was found to explain the observed excess rather nicely [16]. However, the limit on 4τ searches at the LHC [17–22] has subsequently brought in some constraints on the on-shell decay $h \to AA \to 4\tau$. Therefore, it appears more appropriate if m_A is a little above the pair-production threshold in h-decay. Even after respecting this constraint, one still finds [4] a substantial parameter region consistent with the latest result on $(g-2)_\mu$ [6–8,44–46] at the 3σ level. The estimate in [4] includes contributions from two-loop Bar-Zee diagrams, following Refs. [47–49]. Our analysis is based on benchmarks within this region.

Keeping the above discussion in mind, an interesting and at the same time consistent region in the type-X 2HDM parameter space is

$$\frac{m_h}{2} < m_A \lesssim 100\ \text{GeV}, \qquad \tan\beta > 40\ \text{GeV},$$
$$200\ \text{GeV} \lesssim m_H \simeq m_{H^\pm} \lesssim 400\ \text{GeV}.$$

This prompts our four benchmark points tabulated in Table II, for the collider analysis presented in the following sections.

TABLE II. The set of benchmark points chosen for further collider studies. All three points are allowed by the theoretical and experimental constraints described above.

	m_A (GeV)	m_H (GeV)	$m_{H^\pm}$ (GeV)	$\tan\beta$
BP1	63.1	210.7	204.0	61.8
BP2	63.2	249.0	250.2	60.0
BP3	70.2	217.0	213.5	69.8

III. COLLIDER STUDY

A. Signal and background

We consider signals arising out of the hard scattering process $pp \to HA$ and $pp \to H^\pm A$ at the 14 TeV LHC. The fact that m_H and $m_H^\pm$ are constrained to be closely spaced enables us to club together these two hard scattering processes, and analyse the resulting final states with the same kinematic criteria. The dominant decay modes of H or $H^\pm$ are to a massive weak boson Z or $W^\pm$ whereas the pseudoscalar A predominantly decays to a pair of $\tau^\pm$ leptons [50,51]. The weak bosons decay hadronically. Therefore, the following signals ensue from both of the above production channels.

$$pp \to HA \to ZAA \to 4\tau + \text{jets} \tag{16}$$

$$pp \to H^\pm A \to W^\pm AA \to 4\tau + \text{jets} \tag{17}$$

$$pp \to HA \to 4\tau \tag{18}$$

In this way, we finally have $2\tau^+ + 2\tau^- + \text{jets}$ as final states after all the decays cascading from heavy scalars or light pseudoscalars. Being unstable, the τ decays to the other two light leptons with a branching ratio at $\approx 35\%$. However, it has a higher branching ratio of $\approx 65\%$, to jets via hadronic decay modes. These jets formed out of the hadronic decays of τ leptons are usually distinct from light QCD jets due to their low multiplicity in terms of their constituents and therefore can be tagged as τ jets. These jets, usually written as τ_h, have almost 60% tagging efficiency with a very small ($\approx 0.5\%$) mistagging rate [52] defined as the fraction at which the other jets, falsely, are being tagged as τ_h. Even with this relatively high efficiency and really small mistagging rate, the signal in the said channel will tend to be swamped by the QCD background, especially in the regions of the τ-jets having p_T around 10–50 GeV.

We, therefore, propose a subset of the 4τ final state, in which SM backgrounds can be managed better. In order to do so, we make use of the leptonic decay modes of two of the four τ's. Although the branching ratio in this channel is modest, the cleanliness of the lepton detection compensates for its low branching ratio. More precisely, we look for those events where the two leptons for τ-decays are of the same signs. At the same time, two τ-jets of the same sign are tagged, thanks to the high τ-jets charge identification efficiencies in the one-and three-prong channels, as already mentioned [25]. Thus the final state we look at is ($2\ell^\pm + 2\tau_h^\mp + \text{jets}$). A representative Feynman diagram of our signal cascading all the way down to the final signal is illustrated in Fig. 2(a). The SM backgrounds are substantially reduced on demanding the same charges for the τ-jet pair and at the same time for the lepton-pair.

The main backgrounds considered in this analysis are

$$\begin{aligned} pp &\to VV + \text{jets} \\ &\hookrightarrow 2\tau^\pm + 2\tau^\mp + \text{jets} \\ &\hookrightarrow \tau^+\tau^-\ell^\pm\nu_\ell + \text{jets}, \end{aligned} \tag{19}$$

$$pp \to t\bar{t}, \tag{20}$$

$$pp \to t\bar{t}V. \tag{21}$$

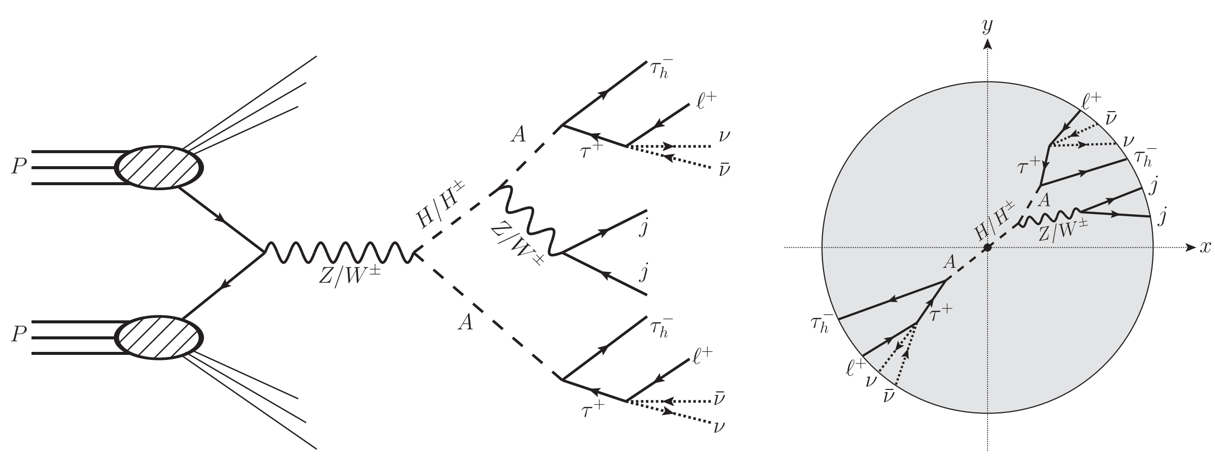

FIG. 2. (a) Representative Feynman diagram for the signal process $pp \to HA$ and $pp \to H^\pm A$ along with the final states after the subsequent cascade decays. (b) Representative schematic diagram of different objects projected in the $x-y$ plane of the collision.

The primary background for the signal comes from $VV+\text{jets}$, where $V=\gamma^*, Z, W^\pm$. In the case of both of the vector bosons being γ^* and Z, it can directly produce $2\tau^\pm + 2\tau^\mp + \text{jets}$, and thereby end up becoming an irreducible background. On the other hand, if one vector boson is $W^\pm$, which decays to leptons and the other V being Z or γ^* decays to $\tau^\pm$ pairs, it can also give rise to two same-sign leptons. In that case, one lepton comes from a W boson and the other comes from a τ. Two same-sign τ's do not come directly. However, a QCD jet mistagged as a τ_h gives rise to two same-sign τ_hs in an event. In our study, we have generated the $VV+\text{jets}$ background events in the two above-mentioned scenarios explicitly, i.e., $pp\to 4\tau+\text{jets}$ and $pp\to 2\tau+W+\text{jets}$. Another set of important background channels turns out to be $t\bar{t}$ and $t\bar{t}V$ because of their large cross sections. One of the same-sign leptons appears from the semileptonic decay of B meson and the other appears directly from the $W^\pm$ decays. We also note that the background $pp\to V+\text{jets}\to\tau^+\tau^-+\text{jets}$ has relatively large cross section. However, its contribution to the final state after requiring the same-sign leptons and τ-jets is found to be negligible, with an efficiency of 10^{-7}. Therefore, $V+$ jets background has not been considered for further analysis.

For the backgrounds, the parton-level events were generated at the leading order (LO) in QCD and QED coupling. Then an appropriate k-factor has been multiplied with the cross section in each of the backgrounds to make up for the correction at the next-to-leading-order (NLO) for $t\bar{t}V$ background, and at the next-to-next-to-leading-order (NNLO) for $VV+\text{jets}$ and $t\bar{t}$ backgrounds. The k-factors are 1.38, 1.57, 1.60, and 2.01, 1.72 for $t\bar{t}Z$ [53], $t\bar{t}W$ [54], $t\bar{t}$ [55], $\tau^+\tau^-W+$ jets [56], and $2\tau^\pm+2\tau^\mp+\text{jets}$ [57], respectively.

Before entering into further discussion on the background reduction strategy, we outline our tools and analysis procedure. The parton-level signal and the background events have been generated using Madgraph5 [58]. These parton-level events have then been showered and hadronized by the PYTHIA8 [59] event generator. We used the fast detector simulator DELPHES [60] for the simulation of detector effects. We employed two separate algorithms for the formation of jets from the DELPHES `eflow` output[2]: (a) standard anti-k_t algorithm (AK) [61] with radius 0.5, and (b) dynamic radius anti-k_t (DR-AK) algorithm [26] recently developed by some of us with an initial radius 0.4. For the tagging of τ-jets, we used the DELPHES τ-tagger with efficiency 0.6 and misidentification efficiency 0.01.

Since the signal is primarily coming from the cascade decay of two particles with masses in the range 60–200 GeV produced in hard scattering, the two same-sign leptons, as well as the two same-sign τ_h's, tend to have large separations in the azimuthal plane as illustrated schematically in Fig. 2(b). This is exhibited in Figs. 3(a) and 3(b) via the distribution of $\Delta\phi(\ell_1,\ell_2)$, where ℓ_1 and ℓ_2 are the p_T-wise leading and subleading leptons, respectively. For both cases, the signals have peaks at $\Delta\phi=\pi$ representative of the mentioned feature for the signal. The combined background is more of a uniform distribution in this variable. A similar feature is seen in Figs. 3(c) and 3(d) for the $\Delta\phi$ between the two same-sign τ-jets. Another important variable H_T, defined as

$$H_T = \sum_{i\in\text{visible}} |\vec{p}_T^{\,i}|, \tag{22}$$

is particularly useful in discriminating signals from the background. The distribution of this variable is plotted in Figs. 3(e) and 3(f). In both AK and DR-AK cases, we can see that the background tends to have higher H_T compared to that of the signals. So, overall, a lower cut on the $\Delta\phi$ between the two same-sign leptons or the two same-sign τ-jets and an upper cut on the variable H_T are useful in separating signals from the backgrounds.

B. Result and discussions

We are now ready to present signal vs. background analyses. For the current study, we performed cut-based analyses with an integrated luminosity of $\mathcal{L}=3000\ \text{fb}^{-1}$. We employed the following set of kinematic acceptance cuts on the DELPHES-generated same-sign leptons, same-sign τ-jets, and QCD jets.

$$\text{Acceptance Cuts}: \begin{cases} p_T^{\ell_1} > 20\ \text{GeV}, \quad p_T^{\ell_2} > 15\ \text{GeV}, \quad |\eta_\ell| < 2.5, \\ p_T^{j} > 30\ \text{GeV}, \quad p_T^{\tau_h} > 30\ \text{GeV}, \quad |\eta_{j,\tau_h}| < 4.7, \\ N_{\ell^\pm} = 2, \quad N_{\tau_h^\mp} = 2, \quad N_j \geq 2, \quad \Delta R(\tau_h,\tau_h) > 0.6. \end{cases} \tag{23}$$

As mentioned previously, we tried two different methods, namely AK and DR-AK algorithms, to cluster the jets from the DELPHES `eflow` outputs. These two algorithms show very similar distributions for the signal and for the backgrounds as shown in Fig. 3.

We have applied lower cuts (as selection cuts) on the $\Delta\phi$ between the two same-sign leptons and between the two same-sign τ-jets. In Table III, we list the details of the cuts and the number of events accepted after the specified cuts for the three benchmark signals and for the backgrounds. As expected from the distribution in $\Delta\phi$ (shown in Fig. 3),

[2]Operationally, the DELPHES-implemented `eflow` outputs are closer to particle flow output at the CMS [60].

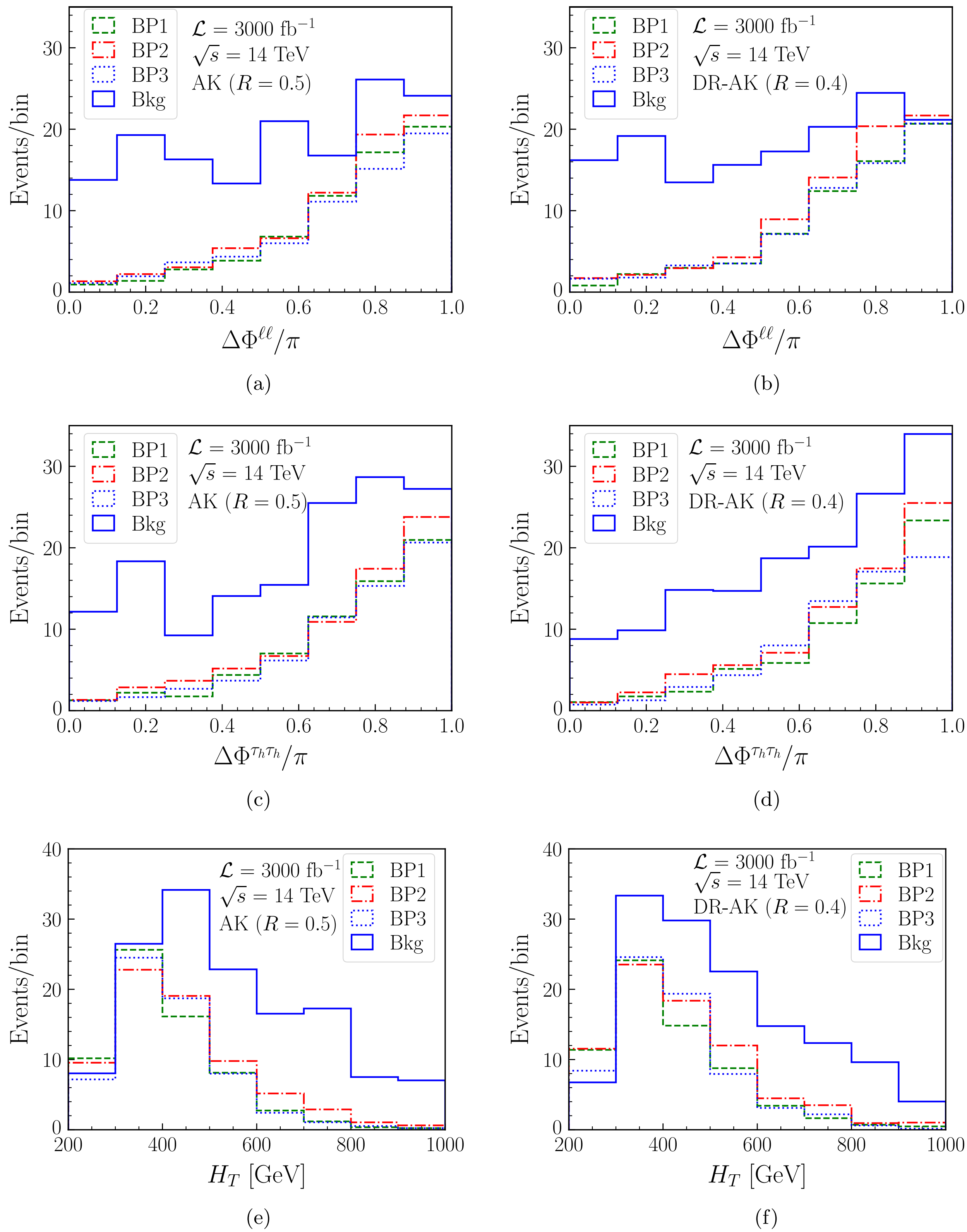

FIG. 3. Distribution in different event variables for signals and backgrounds. The left column is the distribution when the jets are clustered using anti-k_t algorithm with radius $R = 0.5$. The right column is for the dynamic radius anti-k_t algorithm with initial radius $R = 0.4$.

TABLE III. The cut-flow table for the $2\ell^{\pm} + 2\tau^{\mp}$ + jets channel. The number of events after the specified cuts are shown for standard anti-k_t (AK) with radius $R = 0.5$, and dynamic radius anti-k_t (DR-AK) algorithm with initial radius $R = 0.4$ for the signals and backgrounds.

	Number of events at $\mathcal{L} = 3000$ fb^{-1} at $\sqrt{s} = 14$ TeV LHC							
	BP1		BP2		BP3		Backgrounds	
Cuts	AK	DR-AK	AK	DR-AK	AK	DR-AK	AK	DR-AK
Acceptance [Eq. (23)]	65	66	62	66	72	76	138	137
$\Delta\phi(\ell_1, \ell_2) \geq 1.5$	57	56	53	57	60	66	82	78
$\Delta\phi(\tau_1, \tau_2) \geq 1.0$	53	53	49	54	55	61	68	66
$H_T \leq 500$	43	41	40	43	40	44	34	37

the background is reduced by a factor of two whereas the signals are reduced only by 20%. Additionally, the cut on the variable H_T further reduces the total background by another factor of two with less than 10% reduction in the signals.

The collider experiments, in general, are susceptible to systematics uncertainty. In the HL-LHC also, we expect a certain amount of uncertainty. We, therefore, choose to present the signal significance with systematic uncertainties

$$\mathfrak{S} = \sqrt{2}\left[(S+B)\ln\left(1+\frac{S}{B+\epsilon^2 B(S+B)}\right) - \epsilon^{-2}\ln\left(1+\frac{\epsilon^2 S}{1+\epsilon^2 B}\right)\right]^{\frac{1}{2}}, \quad (24)$$

where $B(S)$ are the number of background (signal) events after the selection cuts at a given luminosity and ϵ is the overall systematic uncertainty fraction. We tabulate the signal significance for the three benchmark points in Table IV for four selected systematic uncertainties (5%, 10%, 15%, 20%). The expected signal significance for all the benchmark points is quite good. For all the benchmark points, the significances are approximately 5σ with 10% systematics and are well above 3σ even with 20% systematics, which is moderately high according to the current run of the LHC. The two methods, namely the fixed radius and the dynamic radius anti-k_t algorithm, of forming jets yield almost similar results indicative of the performance of the DR-AK algorithm at per with the traditional AK algorithms.

TABLE IV. The signal significances at the $\sqrt{s} = 14$ TeV LHC at $\mathcal{L} = 3000$ fb^{-1}, for different levels of systematics. The significances are shown for standard anti-k_t (AK) with radius $R = 0.5$, and dynamic radius anti-k_t (DR-AK) algorithm with initial radius $R = 0.4$ for the signals and backgrounds.

	Significance ($\mathfrak{S}$)					
	BP1		BP2		BP3	
Systematics	AK	DR-AK	AK	DR-AK	AK	DR-AK
5%	6.0	5.5	5.6	5.7	5.6	5.8
10%	5.2	4.8	4.9	4.9	4.9	5.0
15%	4.5	4.0	4.1	4.2	4.2	4.2
20%	3.8	3.4	3.5	3.5	3.5	3.6

While the AK algorithm has been in use for quite some time, the DR-AK scheme [26], recently developed by us, has been profitably used in other contexts, especially when the physical origin of jets of differing radii are to be distinguished. As can be seen from Fig. 3 and Tables III and IV, the new algorithm is competitive and in fact performs better in some kinematic regions.

The result presented here is for 3000 fb^{-1} integrated luminosity, for which the signal significance often rises to the discovery level in the $2\ell^{\pm} + 2\tau^{\mp}$ + jets channel. However because of its clean nature, the signal starts having significance exceeding 3σ even at 1000 fb^{-1}, provided the systematics can be brought under sufficient control (within 10%). This is indeed a possibility in the CMS phase-2 detector at the HL-LHC with the improved detector sensitivity in the CMS detectors [62]. Furthermore, with the improved τ-tagging efficiency due to the incorporation of an online L1 tracker trigger [63] at the CMS, finding the signal in our proposed channel can indeed be of high significance.

IV. SUMMARY AND CONCLUSION

Type-X 2HDM is a phenomenologically well-motivated BSM scenario. We have performed a scan over the parameter space of this model, taking into account the constraints coming from the theoretical consistency, measurement of the electroweak oblique parameter at the LEP, and various scalar searches at the LHC. The scalar searches at the LHC constrain the mass of the CP-odd scalar (m_A) to be above $m_h/2$ primarily because of the nonobservation of any significant anomaly in the $h \to 4\tau$ channel. On the other hand, the electroweak oblique parameter measurements prefer a region where $m_H \simeq m_{H^{\pm}}$. The anomalous magnetic moment of the muon prefers low m_A and relatively high $\tan\beta$ regions.

We have chosen three benchmark points consistent with the constraints discussed above to examine clean collider signatures in the channel having two same-sign leptons, two same-sign τ-jets, and at least two jets at the HL-LHC. With the fixed-radius anti-k_t algorithm, we achieve approximately 5σ signal significance with moderate systematics of 10% at 3000 fb^{-1} integrated luminosity. A conservative scenario with 20% systematics is also able to yield more than 3σ signal significance. We have parallelly performed the analysis using recently proposed dynamic radius jet clustering algorithm, which produces similar results as the traditional anti-k_t algorithm and thereby establishing the validity of the proposed algorithm. We further note that the signal is likely to appear even with 1000 fb^{-1} luminosity at the CMS phase-2 detector with the projected improved sensitivity in the tracker and enhanced efficiency in the τ-tagging [62,63].

ACKNOWLEDGMENTS

The authors thank Atri Dey for useful discussions. The authors acknowledge the support of the Kepler Computing facility maintained by the Department of Physical Sciences, IISER Kolkata for various computational needs. S. S. thanks the Council of Scientific & Industrial Research (CSIR), Government of India for financial support.

[1] G. C. Branco, P. M. Ferreira, L. Lavoura, M. N. Rebelo, M. Sher, and J. P. Silva, Theory and phenomenology of two-Higgs-doublet models, Phys. Rep. **516**, 1 (2012).

[2] L. Wang, J. M. Yang, and Y. Zhang, Two-Higgs-doublet models in light of current experiments: A brief review, Commun. Theor. Phys. **74**, 097202 (2022).

[3] G. Bhattacharyya and D. Das, Scalar sector of two-Higgs-doublet models: A minireview, Pramana **87**, 40 (2016).

[4] A. Dey, J. Lahiri, and B. Mukhopadhyaya, Muon g-2 and a type-X two-Higgs-doublet scenario: Some studies in high-scale validity, Phys. Rev. D **106**, 055023 (2022).

[5] N. Ghosh and J. Lahiri, Generalized 2HDM with wrong-sign lepton-Yukawa coupling, in light of $g_\mu - 2$ and lepton flavor violation at the future LHC, Eur. Phys. J. C **81**, 1074 (2021).

[6] Muon g-2 Collaboration, Final report of the muon E821 anomalous magnetic moment measurement at BNL, Phys. Rev. D **73**, 072003 (2006).

[7] Muon g-2 Collaboration, Measurement of the anomalous precession frequency of the muon in the Fermilab Muon $g-2$ Experiment, Phys. Rev. D **103**, 072002 (2021).

[8] Muon g-2 Collaboration, Measurement of the Positive Muon Anomalous Magnetic Moment to 0.46 ppm, Phys. Rev. Lett. **126**, 141801 (2021).

[9] T. Blum, N. Christ, M. Hayakawa, T. Izubuchi, L. Jin, C. Jung, and C. Lehner, Hadronic Light-by-Light Scattering Contribution to the Muon Anomalous Magnetic Moment from Lattice QCD, Phys. Rev. Lett. **124**, 132002 (2020).

[10] S. Borsanyi *et al.*, Leading hadronic contribution to the muon magnetic moment from lattice QCD, Nature (London) **593**, 51 (2021).

[11] M. Cè *et al.*, Window observable for the hadronic vacuum polarization contribution to the muon g-2 from lattice QCD, Phys. Rev. D **106**, 114502 (2022).

[12] Extended Twisted Mass Collaboration, Lattice calculation of the short and intermediate time-distance hadronic vacuum polarization contributions to the muon magnetic moment using twisted-mass fermions, Phys. Rev. D **107**, 074506 (2023).

[13] E.-H. Chao, H. B. Meyer, and J. Parrino, Coordinate-space calculation of the window observable for the hadronic vacuum polarization contribution to $(g-2)\mu$, Phys. Rev. D **107**, 054505 (2023).

[14] A. De Santis *et al.*, Lattice calculation of the R-ratio smeared with Gaussian kernels, Proc. Sci. LATTICE2022 (**2023**) 307.

[15] R. Tomás *et al.*, Operational scenario of first high luminosity LHC run, J. Phys. Conf. Ser. **2420**, 012003 (2023).

[16] A. Jueid, J. Kim, S. Lee, and J. Song, Type-X two-Higgs-doublet model in light of the muon g-2: Confronting Higgs boson and collider data, Phys. Rev. D **104**, 095008 (2021).

[17] CMS Collaboration, Search for an exotic decay of the Higgs boson to a pair of light pseudoscalars in the final state of two muons and two τ leptons in proton-proton collisions at $\sqrt{s} = 13$ TeV, J. High Energy Phys. 11 (2018) 018.

[18] ATLAS Collaboration, Search for Higgs boson decays into a pair of light bosons in the $bb\mu\mu$ final state in pp collision at $\sqrt{s} = 13$ TeV with the ATLAS detector, Phys. Lett. B **790**, 1 (2019).

[19] ATLAS Collaboration, Search for the Higgs boson produced in association with a vector boson and decaying into two spin-zero particles in the $H \to aa \to 4b$ channel in pp collisions at $\sqrt{s} = 13$ TeV with the ATLAS detector, J. High Energy Phys. 10 (2018) 031.

[20] CMS Collaboration, Search for an exotic decay of the Higgs boson to a pair of light pseudoscalars in the final state with two muons and two b quarks in pp collisions at 13 TeV, Phys. Lett. B **795**, 398 (2019).

[21] CMS Collaboration, Search for an exotic decay of the Higgs boson to a pair of light pseudoscalars in the final state with two b quarks and two τ leptons in proton-proton collisions at $\sqrt{s} = 13$ TeV, Phys. Lett. B **785**, 462 (2018).

[22] CMS Collaboration, Search for light pseudoscalar boson pairs produced from decays of the 125 GeV Higgs boson in final states with two muons and two nearby tracks in pp

collisions at $\sqrt{s} = 13$ TeV, Phys. Lett. B **800**, 135087 (2020).
[23] E. J. Chun, S. Dwivedi, T. Mondal, and B. Mukhopadhyaya, Reconstructing a light pseudoscalar in the Type-X Two Higgs doublet model, Phys. Lett. B **774**, 20 (2017).
[24] E. J. Chun, S. Dwivedi, T. Mondal, B. Mukhopadhyaya, and S. K. Rai, Reconstructing heavy Higgs boson masses in a type X two-Higgs-doublet model with a light pseudoscalar particle, Phys. Rev. D **98**, 075008 (2018).
[25] CMS Collaboration, Identification of hadronic tau lepton decays using a deep neural network, J. Instrum. **17**, P07023 (2022).
[26] B. Mukhopadhyaya, T. Samui, and R. K. Singh, Dynamic radius jet clustering algorithm, J. High Energy Phys. 04 (2023) 019.
[27] F. Staub, SARAH, arXiv:0806.0538.
[28] F. Staub, SARAH 4: A tool for (not only SUSY) model builders, Comput. Phys. Commun. **185**, 1773 (2014).
[29] C. Degrande, C. Duhr, B. Fuks, D. Grellscheid, O. Mattelaer, and T. Reiter, UFO—The universal FeynRules output, Comput. Phys. Commun. **183**, 1201 (2012).
[30] W. Porod, SPheno, a program for calculating supersymmetric spectra, SUSY particle decays and SUSY particle production at e^+e^- colliders, Comput. Phys. Commun. **153**, 275 (2003).
[31] W. Porod and F. Staub, SPheno 3.1: Extensions including flavour, CP-phases and models beyond the MSSM, Comput. Phys. Commun. **183**, 2458 (2012).
[32] ATLAS Collaboration, Observation of a new particle in the search for the Standard Model Higgs boson with the ATLAS detector at the LHC, Phys. Lett. B **716**, 1 (2012).
[33] CMS Collaboration, Observation of a new boson at a mass of 125 GeV with the CMS experiment at the LHC, Phys. Lett. B **716**, 30 (2012).
[34] Particle Data Group, Review of particle physics, Prog. Theor. Exp. Phys. **2022**, 083C01 (2022).
[35] I. P. Ivanov, Minkowski space structure of the higgs potential in the two-Higgs-doublet model, Phys. Rev. D **75**, 035001 (2007).
[36] A. Barroso, P. M. Ferreira, I. P. Ivanov, and R. Santos, Metastability bounds on the two Higgs doublet model, J. High Energy Phys. 06 (2013) 045.
[37] B. W. Lee, C. Quigg, and H. B. Thacker, The Strength of Weak Interactions at Very High-Energies and the Higgs Boson Mass, Phys. Rev. Lett. **38**, 883 (1977).
[38] A. Arhrib, Unitarity constraints on scalar parameters of the standard and two Higgs doublets model, arXiv:hep-ph/0012353.
[39] P. Bechtle, S. Heinemeyer, T. Klingl, T. Stefaniak, G. Weiglein, and J. Wittbrodt, HiggsSignals-2: Probing new physics with precision Higgs measurements in the LHC 13 TeV era, Eur. Phys. J. C **81**, 145 (2021).
[40] P. Bechtle, D. Dercks, S. Heinemeyer, T. Klingl, T. Stefaniak, G. Weiglein, and J. Wittbrodt, HiggsBounds-5: Testing Higgs sectors in the LHC 13 TeV era, Eur. Phys. J. C **80**, 1211 (2020).
[41] H. Bahl, T. Biekötter, S. Heinemeyer, C. Li, S. Paasch, G. Weiglein, and J. Wittbrodt, HiggsTools: BSM scalar phenomenology with new versions of HiggsBounds and HiggsSignals, Comput. Phys. Commun. **291**, 108803 (2023).
[42] M. E. Peskin and T. Takeuchi, A New Constraint on a Strongly Interacting Higgs Sector, Phys. Rev. Lett. **65**, 964 (1990).
[43] M. E. Peskin and T. Takeuchi, Estimation of oblique electroweak corrections, Phys. Rev. D **46**, 381 (1992).
[44] S. Iguro, T. Kitahara, M. S. Lang, and M. Takeuchi, Current status of the muon g-2 interpretations within two-Higgs-doublet models, arXiv:2304.09887.
[45] E. J. Chun, Z. Kang, M. Takeuchi, and Y.-L. S. Tsai, LHC τ-rich tests of lepton-specific 2HDM for $(g-2)_\mu$, J. High Energy Phys. 11 (2015) 099.
[46] O. Atkinson, M. Black, C. Englert, A. Lenz, and A. Rusov, MUonE, muon g-2 and electroweak precision constraints within 2HDMs, Phys. Rev. D **106**, 115031 (2022).
[47] F. S. Queiroz and W. Shepherd, New physics contributions to the muon anomalous magnetic moment: A numerical code, Phys. Rev. D **89**, 095024 (2014).
[48] V. Ilisie, New Barr-Zee contributions to $(\mathbf{g-2})_\mu$ in two-Higgs-doublet models, J. High Energy Phys. 04 (2015) 077.
[49] A. Cherchiglia, P. Kneschke, D. Stöckinger, and H. Stöckinger-Kim, The muon magnetic moment in the 2HDM: Complete two-loop result, J. High Energy Phys. 01 (2017) 007.
[50] S. Kanemura, K. Tsumura, and H. Yokoya, Multi-tau-lepton signatures at the LHC in the two Higgs doublet model, Phys. Rev. D **85**, 095001 (2012).
[51] S. Kanemura, K. Tsumura, K. Yagyu, and H. Yokoya, Fingerprinting nonminimal Higgs sectors, Phys. Rev. D **90**, 075001 (2014).
[52] CMS Collaboration, Performance of reconstruction and identification of τ leptons decaying to hadrons and ν_τ in pp collisions at $\sqrt{s} = 13$ TeV, J. Instrum. **13**, P10005 (2018).
[53] A. Kardos, Z. Trocsanyi, and C. Papadopoulos, Top quark pair production in association with a Z-boson at NLO accuracy, Phys. Rev. D **85**, 054015 (2012).
[54] S. von Buddenbrock, R. Ruiz, and B. Mellado, Anatomy of inclusive $t\bar{t}W$ production at hadron colliders, Phys. Lett. B **811**, 135964 (2020).
[55] M. Czakon, P. Fiedler, and A. Mitov, Total Top-Quark Pair-Production Cross Section at Hadron Colliders Through $O(\alpha_S^4)$, Phys. Rev. Lett. **110**, 252004 (2013).
[56] M. Grazzini, S. Kallweit, D. Rathlev, and M. Wiesemann, $W^\pm Z$ production at hadron colliders in NNLO QCD, Phys. Lett. B **761**, 179 (2016).
[57] F. Cascioli, T. Gehrmann, M. Grazzini, S. Kallweit, P. Maierhöfer, A. von Manteuffel, S. Pozzorini, D. Rathlev, L. Tancredi, and E. Weihs, ZZ production at hadron colliders in NNLO QCD, Phys. Lett. B **735**, 311 (2014).
[58] J. Alwall, R. Frederix, S. Frixione, V. Hirschi, F. Maltoni, O. Mattelaer, H.-S. Shao, T. Stelzer, P. Torrielli, and M. Zaro, The automated computation of tree-level and next-to-leading order differential cross sections, and their matching to parton shower simulations, J. High Energy Phys. 07 (2014) 079.
[59] T. Sjöstrand, S. Ask, J. R. Christiansen, R. Corke, N. Desai, P. Ilten, S. Mrenna, S. Prestel, C. O. Rasmussen, and P. Z. Skands, An introduction to PYTHIA 8.2, Comput. Phys. Commun. **191**, 159 (2015).

[60] DELPHES 3 Collaboration, DELPHES 3, A modular framework for fast simulation of a generic collider experiment, J. High Energy Phys. 02 (2014) 057.
[61] M. Cacciari, G. P. Salam, and G. Soyez, The anti-k_t jet clustering algorithm, J. High Energy Phys. 04 (2008) 063.
[62] D. Contardo, M. Klute, J. Mans, L. Silvestris, and J. Butler, Technical proposal for the Phase-II upgrade of the CMS detector, Technical Reports No. CERN-LHCC-2015-010, No. LHCC-P-008, No. CMS-TDR-15-02, Geneva, 2015, 10.17181/CERN.VU8I.D59J.
[63] CMS Collaboration, The Phase-2 upgrade of the CMS level-1 trigger, Technical Reports No. CERN-LHCC-2020-004, No. CMS-TDR-021, CERN, Geneva, 2020, https://cds.cern.ch/record/2714892.